A laboratory based edge-illumination x-ray phase-contrast imaging setup with two-directional sensitivity

Gibril K. Kallon, Michal Wesolowski, Fabio A. Vittoria, Marco Endrizzi, Dario Basta, Thomas P. Millard, Paul C. Diemoz, and Alessandro Olivo

Citation: Applied Physics Letters **107**, 204105 (2015); doi: 10.1063/1.4935983
View online: http://dx.doi.org/10.1063/1.4935983
View Table of Contents: http://scitation.aip.org/content/aip/journal/apl/107/20?ver=pdfcov
Published by the AIP Publishing

A laboratory based edge-illumination x-ray phase-contrast imaging setup with two-directional sensitivity

Gibril K. Kallon,[1] Michal Wesolowski,[2] Fabio A. Vittoria,[1] Marco Endrizzi,[1] Dario Basta,[1] Thomas P. Millard,[1] Paul C. Diemoz,[1] and Alessandro Olivo[1]
[1]*Department of Medical Physics and Biomedical Engineering, University College London, Gower Street, WC1E 6BT London, United Kingdom*
[2]*Department of Medical Imaging, University of Saskatchewan, Saskatoon, Saskatchewan S7N 0W8, Canada*

(Received 11 August 2015; accepted 5 November 2015; published online 17 November 2015)

We report on a preliminary laboratory based x-ray phase-contrast imaging system capable of achieving two-directional phase sensitivity, thanks to the use of L-shaped apertures. We show that in addition to apparent absorption, two-directional differential phase images of an object can be quantitatively retrieved by using only three input images. We also verify that knowledge of the phase derivatives along both directions allows for straightforward phase integration with no streak artefacts, a known problem common to all differential phase techniques. In addition, an analytical method for 2-directional dark field retrieval is proposed and experimentally demonstrated. [http://dx.doi.org/10.1063/1.4935983]

Interest in x-ray phase-contrast imaging (XPCi) has increased over recent years due to its ability to visualise features that would be otherwise invisible in conventional x-ray images. The complex refractive index of an object, $n = 1 - \delta + i\beta$, describes its interaction with x-rays. For some samples, the real part decrement, δ (responsible for refraction) can be up to three orders of magnitude greater than β (which accounts for absorption), thus potentially providing improved image contrast compared to conventional x-ray methods. Numerous techniques have been developed to detect the phase signal, among which are free space propagation (FSP),[1,2] grating interferometry (GI),[3–5] crystal analyser-based approaches,[6,7] and non-interferometric methods such as edge-illumination (EI).[8–10] Many of these methods have been progressively translated from synchrotron facilities and adapted to research laboratories using conventional sources,[11] with the final aim of targeting real-world applications. In this regard, grating interferometry and edge-illumination have proved to be most promising.[5,12,13]

EI is a non-interferometric method that can be performed using synchrotron or conventional x-ray sources without the need for source segmentation. Among its main advantages are its relaxed mask alignment conditions,[14] reduced dose to the sample,[15] lack of source coherence restrictions,[16–18] and achromaticity.[17–19] Fig. 1(a) shows a schematic of a standard one dimensional (1D) EI set-up. The incoming x-ray beam is split by a pre-sample mask M_1 (with linear apertures of period p_1) into a series of non-interfering, physically separated beamlets. The beams partially impinge on the periodically arranged absorbing edges of a detector mask, M_2 (of period p_2), placed close to the detector. The masks are positioned along the optical axis such that $p_2 = p_1 \times m$, where m is the geometric magnification defined as $(Z_1 + Z_2)/Z_1$. In the absence of the sample, the detector mask is held fixed and the pre-sample mask is scanned over one period in the vertical direction to obtain the so-called illumination function (IF),[17,20] which relates the level of intensity measured by each pixel to the physical displacement of each beamlet. This is analogous to the rocking curve in analyser based imaging (ABI).[20]

A refracting sample placed immediately downstream of M_1 changes the proportions of each beam incident upon the exposed part of the pixel, and hence the measured intensity. If two images are taken at two different vertical misalignments of M_1 with respect to M_2, corresponding to opposite sides of the IF, the phase contrast signal is reversed, but the absorption signal remains the same. Therefore, the effects caused by refraction and absorption can be separated by phase retrieval algorithms using only these two images.[17] Note that the above described 1D set-up results in one dimensional sensitivity, which means that this type of EI system is only sensitive to phase shifts in the scanning direction, i.e., perpendicular to the mask septa.[10,17,21] Hence, structures inducing refraction in the orthogonal plane (i.e., parallel to the mask septa, along the x-axis in Fig. 1(a)) are less easily detected.

Single directional phase sensitivity is a typical disadvantage of differential XPCi techniques. In fact, aside from FSP, earlier implementations of all other XPCi techniques were inherently phase sensitive in only one direction, and although in recent years 2-dimensional (2D) implementations of GI have emerged,[22–25] none of these enabled maintaining high phase sensitivity without sectioning or collimating an extended source at the source plane.[26]

In this letter, we describe and test a preliminary implementation of a 2D quantitative EI approach with a polychromatic conventional x-ray tube. The pre-sample and detector masks are test structures consisting of a series of L-shaped apertures (see Fig. 1(b)). This unusual aperture shape was selected so that the EI condition could be realised simultaneously along two orthogonal pixel edges. The 2D masks were fabricated by Creatv Microtech according to an earlier design,[13] and in a previous proof-of concept study conducted

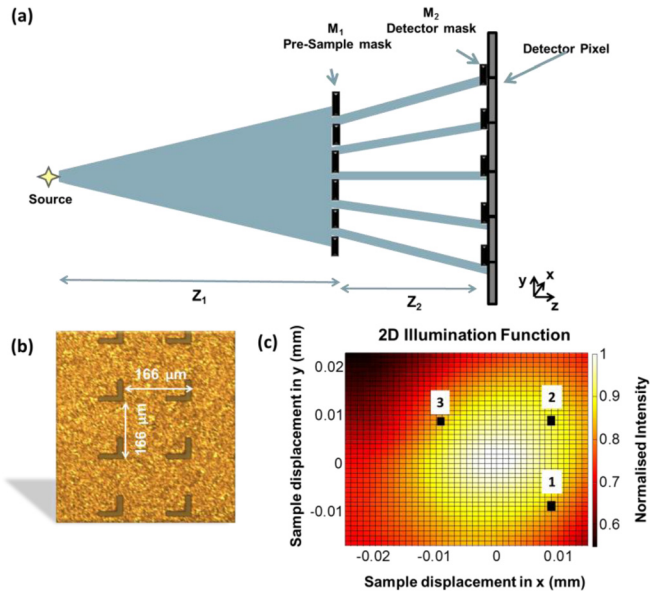

FIG. 1. (a) A standard 1D edge illumination set-up, (b) an optical micrographic image of the 2D detector mask (period = 166 μm), and (c) the illumination function obtained by raster scanning the pre-sample mask (period = 120 μm) with respect to the detector mask. The three imaging positions are indicated on the 2D illumination function.

at a synchrotron were shown to be capable of detecting 2D phase contrast signals without the need to rotate the sample or the imaging system.[27] However, the proof-of-concept nature of this work meant that the first masks were fabricated as thinner ($\sim$30 μm of gold) than their corresponding 1D counterparts, in order to be able to obtain pilot data in a cost-effective manner. This leads to a comparative increase in x-ray transmission through the mask septa, and therefore added background noise to the collected images.

In analogy to the 1D case, the 2D illumination function (Fig. 1(c)) can be acquired in the absence of the sample by raster scanning M_1 with respect to M_2. Given this function, which we call $L(x, y)$, the detected intensity in the presence of a negligibly scattering sample can be described in the following way:

$$I(x, y) = I_T L(x + \Delta x_r; y + \Delta y_r), \tag{1}$$

where I_T is the intensity transmitted through the sample, $\Delta x_r = z_{od}\Delta\theta_{r,x}$ and $\Delta y_r = z_{od}\Delta\theta_{r,y}$ are the lateral shifts suffered by the beam, z_{od} is the object-to-detector distance, and $\Delta\theta_{r,x}$ and $\Delta\theta_{r,y}$ are the refraction angles in the x and y directions, respectively. Making use of the analogy with ABI,[20] we can extend the method developed by Rigon *et al.*[28] and perform a first-order, two-dimensional Taylor expansion, assuming small refraction angles. For the three parameters to be retrieved, i.e., absorption and refraction in x and y, three linearly independent equations can be written using three input images, I_{1-3} acquired at different positions on the IF.

These can be expressed using the following matrix notation:

$$\begin{bmatrix} I_1 \\ I_2 \\ I_3 \end{bmatrix} = \underbrace{I_T \begin{bmatrix} L_1 L_1^x L_1^y \\ L_2 L_2^x L_2^y \\ L_3 L_3^x L_3^y \end{bmatrix}}_{=M} \begin{bmatrix} 1 \\ \Delta x_r \\ \Delta y_r \end{bmatrix}, \tag{2}$$

where L_n^j indicates $\partial L_n/\partial j$ at positions $n = 1, 2, 3$.

The linear system in Eq. (2) can then be solved analytically to retrieve the three images I_T, $\Delta\theta_{r,x}$, and $\Delta\theta_{r,y}$,

$$I_T = \frac{I_1\left(L_2^x L_3^y - L_3^x L_2^y\right) + I_2\left(L_3^x L_1^y - L_1^x L_3^y\right) + I_3\left(L_1^x L_2^y - L_2^x L_1^y\right)}{\det(M)}, \tag{3}$$

$$\Delta\theta_{r,x} = \frac{\Delta x_r}{z_{od}} = \frac{I_1\left(L_3 L_2^y - L_2 L_3^y\right) + I_2\left(L_1 L_3^y - L_3 L_1^y\right) + I_3\left(L_2 L_1^y - L_1 L_2^y\right)}{I_T \det(M)}, \tag{4}$$

$$\Delta\theta_{r,y} = \frac{\Delta y_r}{z_{od}} = \frac{I_1\left(L_2 L_3^y - L_3 L_2^x\right) + I_2\left(L_3 L_1^x - L_1 L_3^x\right) + I_3\left(L_1 L_2^x - L_2 L_1^x\right)}{I_T \det(M)}. \tag{5}$$

Equations (3)–(5) impose no restrictions on the positions at which the images are acquired so long as the three equations are linearly independent.[28] However, since even small angles violate the linear approximation at the peak of the IF, and previous studies, both in ABI[28] and in EI,[17] have shown that certain positions allow for a much improved signal-to-noise ratio (SNR), mixed intensity images were only acquired on linear regions of the IF.

Experimental verification of the proposed method was performed using a rotating anode, Mo-target source (Rigaku 007HF) operated at 35/25 kVp/mA with focal spot full-width at half maximum (FWHM) dimensions of 100 μm in y and 70 μm in x. The amorphous selenium Anrad SMAM flat panel detector was used, which has a pixel size of 85 μm. Both masks were skipped[29] (illuminating every other pixel in order to reduce cross-talk effects), with $p_1 = 120$ μm and $p_2 = 166$ μm, and aperture sizes of 11 and 15 μm, respectively. The absorbing regions consist of a 30 μm layer of gold electroplated upon a 500 μm thick graphite substrate.

The two L-shaped masks M_1 and M_2 were aligned with the detector pixels along the optical axis and were placed at 1.44 m and 1.99 m from the source, respectively. To obtain the experimental 2D-IF shown in Fig. 1(c), the pre-sample mask was scanned (with the detector mask held fixed) over a span of 40 μm in 8 μm steps in x and 5 μm steps in y. The pre-sample mask was then placed at the three different imaging positions shown in Fig. 1(c), where images of a pair of crossed PMMA cylinders (radii 1.5 $\pm$ 0.3 mm) were acquired. It must be noted that the spatial resolution of each image was improved via dithering, i.e., scanning the sample with 6 $\times$ 6 sub-pixel steps of 20 μm, with an exposure time of 10 s per dithering step. Eqs. (3)–(5) were then used to perform the phase retrieval; the results are displayed in Fig. 2.

Fig. 2(a) shows the retrieved transmission image, whilst Figs. 2(b) and 2(c) represent the retrieved refraction angle images in the two orthogonal directions at the sample plane. Furthermore, Figs. 2(d)–2(f) show a good agreement between the experimentally measured and theoretical profiles for the "apparent absorption" and refraction images of the PMMA

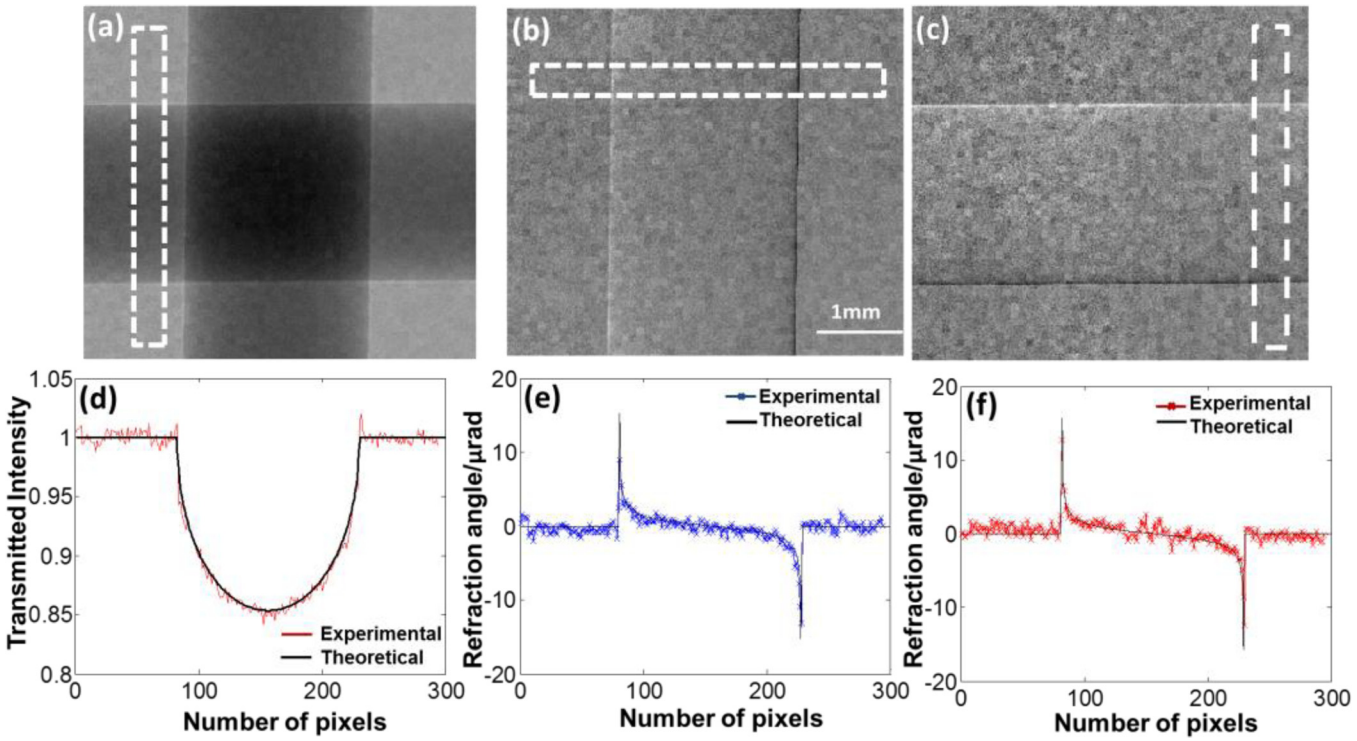

FIG. 2. Retrieved images for two crossed PMMA cylinders: (a) transmission, (b) refraction image along the horizontal direction, and (c) refraction image along the vertical direction. Comparisons between the experimental and theoretical profiles are shown for (d) transmission, (e) refraction along the horizontal direction, and (f) refraction along the vertical direction.

cylinders, demonstrating the approach's quantitativeness. The peaks present at the very edges of the experimental profile of the cylinder in Fig. 2(d) represent a phase enhancement which exists because the slowly varying phase assumption of the algorithm is not satisfied at the very edges of an object.[30] It is worth noting that the horizontal and vertical wires disappear in Figs. 2(b) and 2(c), respectively, since they induce refraction only along the "non-retrieved" direction.

While a direct 1D integration of either refraction image would yield the phase of that object, this is usually accompanied by severe streak artefacts (see supplementary material).[23,31,32] Moreover, in cases where the boundary conditions are not known, e.g., when the object is larger than the field of view, 1D phase integration may not be possible. However, Arnison *et al.*[31] and Kottler *et al.*[23] have demonstrated that the two differential phase images can be combined in Fourier space to retrieve the phase $\Phi(x, y)$, without unfavourable artefacts and regardless of the boundary conditions. This is achieved by performing the Fourier transform of the complex sum of the two differential phase images in Fourier space, dividing it by their spatial frequencies (k, l) and then taking the inverse Fourier transform

$$\Phi(x,y) = \mathcal{F}^{-1}\left[\frac{\mathcal{F}\left[I_{\theta_{r,x}} + iI_{\theta_{r,y}}\right]}{2\pi(k+il)}\right](x,y). \qquad (6)$$

An image of the integrated phase $\Phi(x, y)$, calculated using Figs. 2(b) and 2(c), is shown in Fig. 3(a), and the average phase retrieved profiles are displayed in Figs. 3(b) and 3(c). While mitigating the streak artefacts common to 1D phase integration, the image suffers from some low frequency artefacts, which can potentially arise from an asymmetry in the differential phase profile. It has been shown by Hagen *et al.* that this asymmetry can be caused by the undersampling of an object.[33] Furthermore, the denominator in Eq. (6) acts as a high frequency filter in Fourier space, which amplifies low frequencies and has been known to impose an artificial background on the image.[34] In fact, the presence of these artefacts is a well-known problem in phase integration and has been treated by Langer *et al.*[35] These can be removed by using a priori information of the sample geometry, or using a regularization-based algorithm.[36]

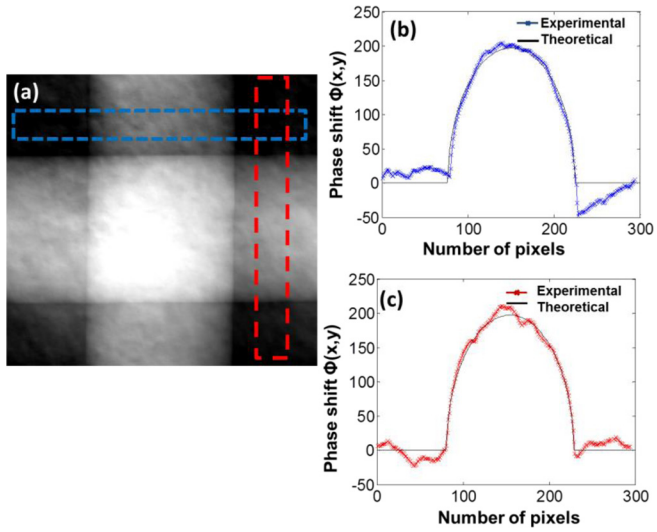

FIG. 3. (a) Integrated phase image of the crossed PMMA cylinders calculated using the Fourier method on the two differential phase images in Figs. 2(b) and 2(c). (b) and (c) show the average horizontal and vertical integrated phase profiles extracted from the regions shown in (a), respectively.

Furthermore, the developed method can be extended to retrieve the two-directional ultra-small angle x-ray scattering (USAXS) images. Scattering is assumed to be a stochastic process taking place at the sub-pixel scale. A full probability distribution of scattering angles $S(\Delta\theta_{s,x,y})$ is assumed to be collected at each pixel and can be modelled as a normalised Gaussian centred at zero,[28,37] i.e., $\int S(\Delta\theta_{s,x,y})d(\Delta\theta_s) = 1$, and $\int(\Delta\theta_s)S(\Delta\theta_{s,x,y})d(\Delta\theta_s) = 0$. The width of the distribution is represented by its standard deviation, $\sigma^2_{\Delta\theta_{s,x,y}}(x,y) = \int(\Delta\theta_s)^2 S(\Delta\theta_{s,x,y})d(\Delta\theta_s)$,[37] and physically manifests as a broadening of the beam after the sample due to scattering. Although the choice of a Gaussian function may be seen as somewhat arbitrary, since several other non-Gaussian functions could be used to model the scattering function, our work on 1D EI has shown that, at least to first approximation, a Gaussian function can be used to fit the retrieved scattering function.[14] For this reason, and especially considering the preliminary nature of this investigation, we have simply extended that treatment to the 2D case.

In the presence of scattering and refraction, a 2D second-order Taylor expansion can be used to describe the effects on the measured intensity

$$I_n = I_T\left[L_n + L_n^x\Delta x_r + L_n^y\Delta y_r + \left(L_n^{xx}\underbrace{\frac{1}{2}\left(\Delta x_r^2 + \sigma_x^2\right)}_{x_{s,r}} + L_n^{yy}\underbrace{\frac{1}{2}\left(\Delta y_r^2 + \sigma_y^2\right)}_{y_{s,r}} + L_n^{xy}\Delta x_r\Delta y_r\right)\right], \tag{7}$$

where $L_n^{j,k}$ indicates $\partial^2 L_n/\partial j\partial k$ at $n = 1-6$ positions about the centre of the illumination function.

The first three terms within the brackets in Eq. (7) have the same meaning as those shown in Eq. (1); in addition, $\sigma_x = z_{od}\sigma_{\Delta\theta_{s,x}}$ and $\sigma_y = z_{od}\sigma_{\Delta\theta_{s,y}}$ are the apparent shifts of the illumination function, which arise due to its broadening, as a result of scattering. Note that σ_x is a distance while $\sigma_{\Delta\theta_{s,x,y}}$ represents an angle. There are five unknowns to retrieve, but in order to derive an analytical solution, we treat the final term as an additional independent variable, thus imposing the need for six input images. The system can then be solved in a similar manner as Eq. (2), which enables the extraction of the two-directional scattering quantities

$$\sigma^2_{\Delta\theta_{s,x}} = \left(\frac{\sigma_x}{z_{od}}\right)^2 = \frac{2x_{s,r} - (\Delta x_r)^2}{z_{od}^2}, \tag{8}$$

$$\sigma^2_{\Delta\theta_{s,y}} = \left(\frac{\sigma_y}{z_{od}}\right)^2 = \frac{2y_{s,r} - (\Delta y_r)^2}{z_{od}^2}. \tag{9}$$

The relation between the final mixed term and the previous ones in Eq. (7) can be used to develop an approach where only 5 input images are required instead of 6, and this will be explored in future developments. In order to experimentally validate the above retrieval method for scattering, an additional experiment was performed with two orthogonally overlapped pieces of wood. Using Eqs. (7)–(9), the "apparent absorption," 2-directional refraction, and scattering images were retrieved and are displayed in Fig. 4. Figs. 4(a)–4(c) show the transmission and refraction images, while Figs. 4(d) and 4(e) show a map of the distribution of the sample's scattering angles in the x and y directions, respectively. Fig. 4(a) shows more phase enhancement along x than along y; this can be attributed to the difference in the source size along the respective directions. In fact, the difference in source size has been shown to lead to different differential phase sensitivities.[17] The wood's microstructure is highly anisotropic, possessing features orientated along preferential directions; thus, the two orthogonal pieces of wood appear differently in images depicting the refraction and scattering along the horizontal and vertical directions, respectively. In particular, the horizontal structures tend to disappear in Figs. 4(b) and 4(d), while the same occurs for the vertical structures in Figs. 4(c) and 4(e). Fig. 4(f) shows the phase retrieved image of the crossed wooden splints, which was calculated by using the two differential phase images in Figs. 4(b) and 4(c) and Eq. (6).

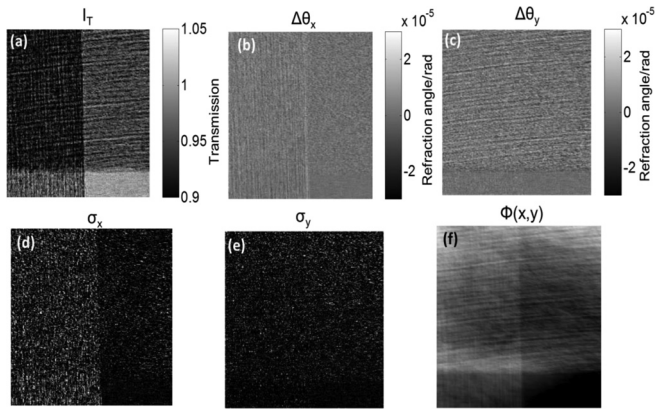

FIG. 4. Retrieved images for a pair of wooden splints for (a) transmission, (b) refraction along the horizontal direction, (c) refraction along the vertical direction, (d), scattering along the horizontal direction, (e) scattering along the vertical direction, and (f) the phase image calculated from the two refraction images (b) and (c).

In conclusion, we described a laboratory implementation of the EI XPCi technique capable of achieving 2D phase and dark field sensitivity using a conventional x-ray source. By exploiting the similarity of the physical principles between ABI and EI, we developed an algorithm that resolves the refraction and scattering signals in both directions, and proved the quantitativeness of the technique. In addition, the possibility of obtaining a map of the sample phase from a combination of the two-directional differential phase images was demonstrated, which effectively eliminates the streak artefacts typically encountered from direct integration of the 1D differential phase image. The method also lends itself naturally to more sophisticated dark-field analysis approaches, like those recently proposed by Modregger *et al.*,[38] which again will be the subject of future investigations.

This work was supported by the UK Engineering and Physical Sciences Research Council Grant No. EP/I021884/1 and by the UK Science and Technology Facilities Council Grant No. ST/L502662/1. P.C.D. and M.E. are supported by Marie Curie Career Integration Grants within the Seventh Framework Programme of the European Union, PCIG12-

GA-2012-333990/334056, and M.W. was supported by the Burroughs Wellcome Collaborative research Travel Grant No. 1014038.

[1]A. Snigirev, I. Snigireva, V. Kohn, S. Kuznetsov, and I. Schelokov, "On the possibilities of x-ray phase contrast microimaging by coherent high-energy synchrotron radiation," Rev. Sci. Instrum. **66**, 5486–5492 (1995).
[2]P. Cloetens, R. Barrett, J. Baruchel, J. P. Guigay, and M. Schlenker, "Phase objects in synchrotron radiation hard x-ray imaging," J. Phys. D: Appl. Phys. **29**, 133–146 (1996).
[3]A. Momose, S. Kawamoto, I. Koyama, Y. Hamaishi, K. Takai, and Y. Suzuki, "Demonstration of x-ray Talbot interferometry," Jpn. J. Appl. Phys., Part 2: Lett. **42**, L866 (2003).
[4]T. Weitkamp, A. Diaz, C. David, F. Pfeiffer, M. Stampanoni, P. Cloetens, and E. Ziegler, "X-ray phase imaging with a grating interferometer," Opt. Express **13**, 6296–6304 (2005).
[5]F. Pfeiffer, T. Weitkamp, O. Bunk, and C. David, "Phase retrieval and differential phase-contrast imaging with low-brilliance X-ray sources," Nat. Phys. **2**, 258–261 (2006).
[6]T. J. Davis, D. Gao, T. E. Gureyev, A. W. Stevenson, and S. W. Wilkins, "Phase-contrast imaging of weakly absorbing materials using hard X-rays," Nature **373**, 595–598 (1995).
[7]D. Chapman, W. Thomlinson, R. E. Johnston, D. Washburn, E. Pisano, N. Gmür, Z. Zhong, R. Menk, F. Arfelli, and D. Sayers, "Diffraction enhanced x-ray imaging," Phys. Med. Biol. **42**, 2015–2025 (1997).
[8]A. Olivo, F. Arfelli, G. Cantatore, R. Longo, R. H. Menk, S. Pani, M. Prest, P. Poropat, L. Rigon, G. Tromba, E. Vallazza, and E. Castelli, "An innovative digital imaging set-up allowing a low-dose approach to phase contrast applications in the medical field," Med. Phys. **28**, 1610–1619 (2001).
[9]A. Olivo, K. Ignatyev, P. R. T. Munro, and R. D. Speller, "Noninterferometric phase-contrast images obtained with incoherent x-ray sources," Appl. Opt. **50**, 1765–1769 (2011).
[10]P. R. T. Munro, K. Ignatyev, R. D. Speller, and A. Olivo, "Phase and absorption retrieval using incoherent X-ray sources," Proc. Natl. Acad. Sci. **109**, 13922–13927 (2012).
[11]A. Olivo and I. Robinson, "Taking X-ray phase contrast imaging into mainstream applications' and its satellite workshop 'Real and reciprocal space X-ray imaging'," Philos. Trans. R. Soc. A **372**, 20130359 (2014).
[12]J. Zambelli, N. Bevins, Z. Qi, and G. H. Chen, "Radiation dose efficiency comparison between differential phase contrast CT and conventional absorption CT," Med. Phys. **37**, 2473–2479 (2010).
[13]P. Munro, K. Ignatyev, R. Speller, and A. Olivo, "Design of a novel phase contrast X-ray imaging system for mammography," Phys. Med. Biol. **55**, 4169–4185 (2011).
[14]T. P. Millard, M. Endrizzi, K. Ignatyev, C. K. Hagen, P. R. T. Munro, R. D. Speller, and A. Olivo, "Method for automatization of the alignment of a laboratory based x-ray phase contrast edge illumination system," Rev. Sci. Instrum. **84**, 083702 (2013).
[15]T. P. Millard, M. Endrizzi, P. C. Diemoz, C. K. Hagen, and A. Olivo, "Monte Carlo model of a polychromatic laboratory based edge illumination x-ray phase contrast system," Rev. Sci. Instrum. **85**, 053702 (2014).
[16]A. Olivo and R. Speller, "A coded-aperture technique allowing x-ray phase contrast imaging with conventional sources," Appl. Phys. Lett. **91**, 074106 (2007).
[17]P. C. Diemoz, C. K. Hagen, M. Endrizzi, and A. Olivo, "Sensitivity of laboratory based implementations of edge illumination X-ray phase-contrast imaging," Appl. Phys. Lett. **103**, 244104 (2013).
[18]P. C. Diemoz and A. Olivo, "On the origin of contrast in edge illumination X-ray phase-contrast imaging," Opt. Express **22**, 28199–28214 (2014).
[19]M. Endrizzi, F. A. Vittoria, G. Kallon, D. Basta, P. C. Diemoz, A. Vincenzi, P. Delogu, R. Bellazzini, and A. Olivo, "Achromatic approach to phase-based multi-modal imaging with conventional X-ray sources," Opt. Express **23**, 16473 (2015).
[20]P. R. T. Munro, C. K. Hagen, M. B. Szafraniec, and A. Olivo, "A simplified approach to quantitative coded aperture X-ray phase imaging," Opt. Express **21**, 11187–11201 (2013).
[21]M. Endrizzi, P. C. Diemoz, T. P. Millard, J. Louise Jones, R. D. Speller, I. K. Robinson, and A. Olivo, "Hard X-ray dark-field imaging with incoherent sample illumination," Appl. Phys. Lett. **104**, 024106 (2014).
[22]I. Zanette, T. Weitkamp, T. Donath, S. Rutishauser, and C. David, "Two-dimensional X-ray grating interferometer," Phys. Rev. Lett. **105**, 2–5 (2010).
[23]C. Kottler, C. David, F. Pfeiffer, and O. Bunk, "A two-directional approach for grating based differential phase contrast imaging using hard x-rays," Opt. Express **15**, 1175–1181 (2007).
[24]K. Nagai, "A phase demodulation method for two-dimensional grating-based X-ray interferometry," Philos. Trans. R. Soc. A Math. Phys. Eng. Sci. **372**, 20130034 (2014).
[25]H. H. Wen, E. E. Bennett, R. Kopace, A. F. Stein, and V. Pai, "Single-shot x-ray differential phase-contrast and diffraction imaging using two-dimensional transmission gratings," Opt. Lett. **35**, 1932–1934 (2010).
[26]G. Sato, T. Kondoh, H. Itoh, S. Handa, K. Yamaguchi, T. Nakamura, K. Nagai, C. Ouchi, T. Teshima, Y. Setomoto, and T. Den, "Two-dimensional gratings-based phase-contrast imaging using a conventional x-ray tube," Opt. Lett. **36**, 3551–3553 (2011).
[27]A. Olivo, S. E. Bohndiek, J. A. Griffiths, A. Konstantinidis, and R. D. Speller, "A non-free-space propagation x-ray phase contrast imaging method sensitive to phase effects in two directions simultaneously," Appl. Phys. Lett. **94**, 044108 (2009).
[28]L. Rigon, F. Arfelli, and R. H. Menk, "Generalized diffraction enhanced imaging to retrieve absorption, refraction and scattering effects," J. Phys. D. Appl. Phys. **40**, 3077–3089 (2007).
[29]K. Ignatyev, P. R. T. Munro, R. D. Speller, and A. Olivo, "Effects of signal diffusion on x-ray phase contrast images," Rev. Sci. Instrum. **82**, 073702 (2011).
[30]O. Oltulu, Z. Zhong, M. Hasnah, M. N. Wernick, and D. Chapman, "Extraction of extinction, refraction and absorption properties in diffraction enhanced imaging," J. Phys. D: Appl. Phys. **36**, 2152–2156 (2003).
[31]M. R. Arnison, K. G. Larkin, C. J. R. Sheppard, N. I. Smith, and C. J. Cogswell, "Linear phase imaging using differential interference contrast microscopy," J. Microsc. **214**, 7–12 (2004).
[32]See supplementary material at http://dx.doi.org/10.1063/1.4935983 for the two, one-dimensionally retrieved phase integrated images of the vertcial and horizontal cylinders that are shown in the text, respectively.
[33]C. K. Hagen, P. C. Diemoz, M. Endrizzi, and A. Olivo, "The effect of the spatial sampling rate on quantitative phase information extracted from planar and tomographic edge illumination x-ray phase contrast images," J. Phys. D: Appl. Phys. **47**, 455401 (2014).
[34]K. Scherer, L. Birnbacher, M. Chabior, J. Herzen, D. Mayr, S. Grandl, A. Sztrókay-Gaul, K. Hellerhoff, F. Bamberg, and F. Pfeiffer, "Bi-directional x-ray phase-contrast mammography," PLoS One **9**, e93502 (2014).
[35]M. Langer, P. Cloetens, and F. Peyrin, "Regularization of phase retrieval with phase-attenuation duality prior for 3-D holotomography," IEEE Trans. Image Process. **19**, 2428–2436 (2010).
[36]I. Zanette, T. Zhou, A. Burvall, U. Lundström, D. H. Larsson, M. Zdora, P. Thibault, F. Pfeiffer, and H. M. Hertz, "Speckle-based X-ray phase-contrast and dark-field imaging with a laboratory source," Phys. Rev. Lett. **112**(25), 253903 (2014).
[37]L. Rigon, H. J. Besch, F. Arfelli, R. H. Menk, G. Heitner, and H. Plothow-Besch, "A new DEI algorithm capable of investigating sub-pixel structures," J. Phys. D: Appl. Phys. **36**, A107–A112 (2003).
[38]P. Modregger, S. Rutishauser, J. Meiser, C. David, and M. Stampanoni, "Two-dimensional ultra-small angle X-ray scattering with grating interferometry," Appl. Phys. Lett. **105**, 024102 (2014).